Correspondence to:
D. Beletsky,
beletsky@umich.edu

Modeling a Large Coastal Upwelling Event in Lake Superior

Yaru Li[1,2,3] , **Dmitry Beletsky**[3] , **Jia Wang**[4] , **Jay Austin**[5], **James Kessler**[4], **Ayumi Fujisaki-Manome**[3,6] , **and Peng Bai**[4]

[1]North China Sea Marine Forecasting Center, Oceanic Administration of China, Qingdao, China, [2]Shandong Provincial Key Laboratory of Marine Ecological Environment and Disaster Prevention and Mitigation, Qingdao, China, [3]Cooperative Institute for Great Lakes Research, University of Michigan, Ann Arbor, MI, USA, [4]Great Lakes Environmental Research Laboratory, Office of Oceanic and Atmospheric Research, National Oceanic and Atmospheric Administration, Ann Arbor, MI, USA, [5]Large Lakes Observatory and Department of Physics and Astronomy, University of Minnesota-Duluth, Duluth, MN, USA, [6]Climate & Space Sciences and Engineering, University of Michigan, Ann Arbor, MI, USA

Abstract An extraordinary strong wind-driven upwelling event occurred in Lake Superior in summer of 2010 when the lake was strongly stratified. In this paper, a detailed three-dimensional (3-D) investigation of the current and thermal structures during the upwelling event was conducted using in situ observations, remote sensing products, and the results of a long-term numerical simulation. A 3-D finite-volume coupled ice–ocean model tailored for the Laurentian Great Lakes was employed for this purpose. The model was validated with temperature observations at National Oceanic and Atmospheric Administration buoys and mooring data from 2010. The upwelling event observed in satellite imagery and at a mooring station was reproduced by the model, showing a cooling of as much as 10°C in August 2010 along the northwestern coast. The relationship between the alongshore wind and the offshore thermocline displacement (upwelling front) derived in theoretical work (Csanady, 1977, https://doi.org/10.1029/JC082i003p00397) was used to calculate upwelling front movement offshore and found to be in in close agreement with model prediction. A significant correlation between alongshore wind stress and lake temperature change in the upwelling zone was found with a correlation coefficient of −0.87. A simple linear heat balance model explained most of variability in temperature.

Plain Language Summary An extraordinary strong upwelling event observed during summer 2010 in Lake Superior was reproduced by a numerical ocean model. A detailed three-dimensional (3-D) investigation of the current and thermal structures during the upwelling event was conducted using in situ observations, remote sensing products, and the results of a long-term numerical simulation. A 4-day long strong, persistent alongshore wind was the major driving force of this event. A significant correlation between alongshore wind stress and lake temperature change in the upwelling zone was found. A simple linear heat balance model explained most of variability in temperature measurements. The relationship between the alongshore wind and the offshore displacement of the upwelling front derived in theoretical work was used to calculate upwelling front movement offshore and found to be in in close agreement with model prediction.

1. Introduction

Coastal upwelling and downwelling is frequently observed in the ocean and large lakes (Austin & Lentz, 2002; Csanady, 1977; Smith, 1995). Driven by alongshore surface winds and the resulting Ekman transports, coastal upwelling is characterized by water mass transport between onshore and offshore areas (Brink, 2016) and resulting strong vertical movement. Upwelling caused by strong wind events plays a significant role in heat and momentum transfer at the water–air interface and within the water body and therefore has implications in the evolution of the water thermal structure, as well as the transport and distribution of pollutants, sediment and nutrients in the water body (Austin & Barth, 2002; Beletsky et al., 1997; Csanady, 1977; Plattner et al., 2006; Simons & Schertzer, 1987). Importantly, upwelling events can modify lake stratification, which is closely related to the carbon contribution of lakes to the global carbon cycle (Kirillin & Shatwell, 2016). In oceans, upwelling is acknowledged as the basis of coastal food

webs and carbon fixation, as it brings deep, nutrient-rich water into the euphotic zone. Therefore, coastal upwelling is of fundamental importance to understanding the role of lake dynamics in the physical, biological, ecological, and societal aspects.
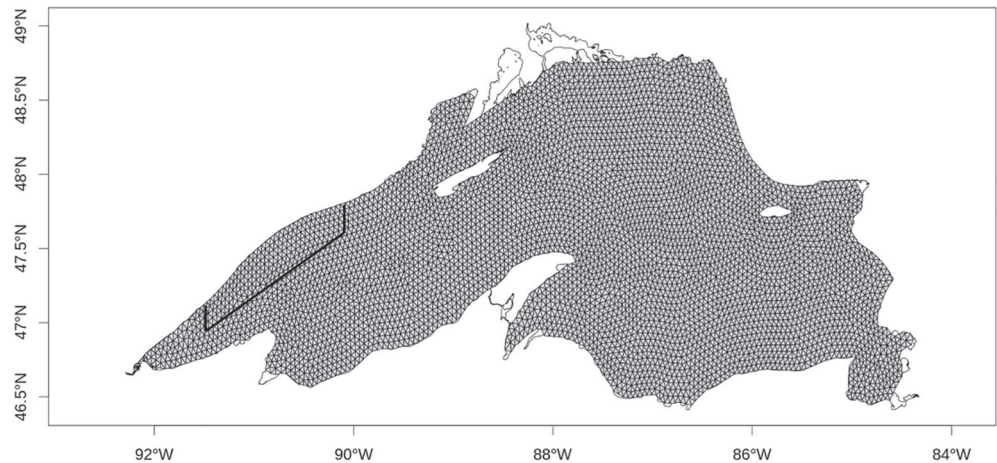
Upwelling studies require information on the thermal structure and currents, yet reliable, long, and continuous records of temperature in lakes are rather rare (Austin & Colman, 2008; Titze & Austin, 2014); data on currents, even more so. It is very difficult to collect enough in situ data with sufficient temporal and spatial resolution to study the thermal structure and upwelling events based on in situ observations alone. However, we can improve our understanding through remote sensing and modeling. Csanady (1977) developed an analytical model predicting the shape of the thermocline during upwelling and the offshore displacement of the upwelling front, which produced reasonably accurate results in the early stages of several upwelling events in Lake Ontario. Among the early numerical modeling attempts in freshwater, Beletsky et al. (1997) applied two numerical ocean models to Lake Michigan and studied a large coastal upwelling event that took place in 1955 (Ayers, 1956). Many recent studies have used a variety of models (Bai et al., 2013; Chen et al., 2001, 2002; White et al., 2012; Ye et al., 2019; Zhu et al., 2001) to advance knowledge of temperature structure and lake circulation drivers. Plattner et al. (2006) used remote sensing data, such as surface temperature images derived from the Advanced Very High Resolution Radiometer (AVHRR) and wind data from buoys, to show a relationship between upwelling events and wind directions along the western and eastern shorelines of Lake Michigan.

The general circulation and thermal structure in Lake Superior has been studied much less intensively than the other Great Lakes, like Lake Michigan and Lake Erie, and many studies addressed the issue in a climatological manner (Bai et al., 2013; Beletsky et al., 1999; Bennington et al., 2010). Studies focusing on upwelling events in Lake Superior have received sparse attention apart from a few studies focusing on the Keweenaw Current area (Niebauer et al., 1977). In particular, Niebauer et al. (1977) studied the current, hydrographic, and wind data in the Keweenaw Current area in Lake Superior and arrived at a conclusion that the coastal upwelling and offshore Ekman transport were generated by alongshore winds associated with migrating high-pressure systems. More recently, long-term observations of temperature at several locations across the lake were initiated (Austin, 2013), allowing the study of the evolution of thermal structure on a variety of time scales, including hourly-daily time scales, which are relevant for wind-driven upwelling. In this paper, we take advantage of this new and rich data set, which is complemented by remotely sensed data and the results of multiyear modeling. We focus on the summer of 2010, when the lake was strongly stratified and a series of upwelling-favorable wind events produced rapid and dramatic changes in lake thermal structure, leading to a full upwelling, in which the bottom layer surfaces (Monismith, 1986). Events of that magnitude in large lakes are rare (Roberts et al., 2021; Schladow et al., 2004), and due to their impact on not only lake physics but chemistry and biology as well, they certainly deserve to be investigated.

In this paper, we investigate this uncommonly strong upwelling event and analyze it in detail. We use measurements from buoys and satellites to validate the model and facilitate our understanding. The structure of the paper is as follows: the numerical model and observational data are described in Sections 2 and 3, respectively. Model results and validation are presented in Section 4. Discussion of model results and comparison with previous theoretical work by Csanady (1977) is presented in Section 5, followed by conclusions in Section 6.

2. Numerical Model

The numerical model used is the spherical coordinate Great Lakes Finite Volume Community Ocean Model (GL-FVCOM) implemented by Bai et al. (2013), which is based on the unstructured-grid finite-volume coastal ocean model FVCOM developed and upgraded by Chen et al. (2003, 2006, 2013). Using a finite-volume approach, FVCOM solves the primitive equations in flux forms with a mode splitting method. The vertically integrated transport equations, where the water elevation is solved explicitly using a short time step, are solved in the external mode, while the 3-D governing equations are solved in the internal mode using a long time step. Unstructured triangular elements in the horizontal are combined with a σ-coordinate scheme vertically to generate a 3-D computational domain, which is simulated with spatially varying Coriolis force. The Smagorinsky turbulent closure schemes (Smagorinsky, 1963) and the modified Mellor and
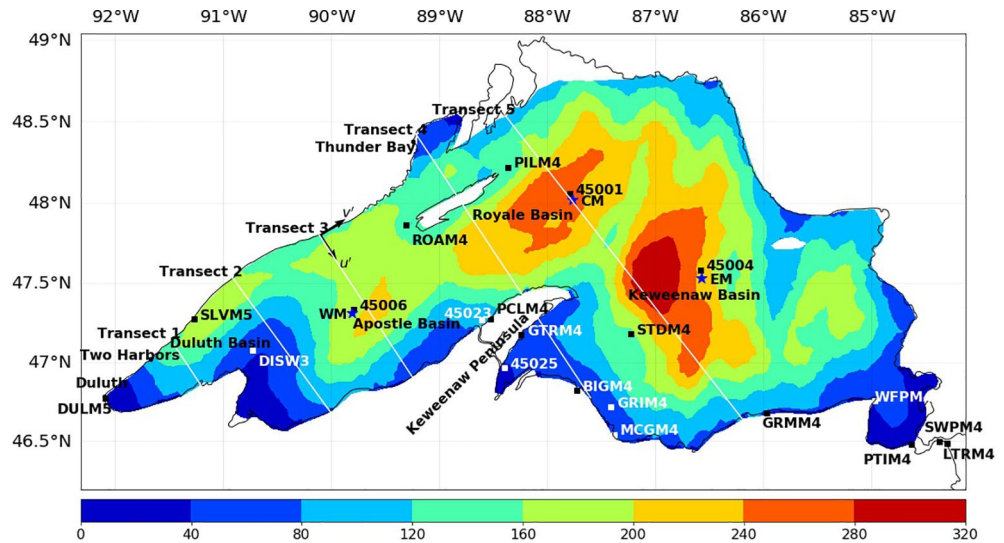
Figure 1. Computational grid for Lake Superior. (Location for a selected upwelling zone is shown by the heavy black lines off the northwestern coast.).

Yamada level 2.5b (MY-2.5) (Mellor & Blumberg, 2004; Mellor, 2001; Mellor & Yamada, 1982) are adopted in the model for the horizontal and vertical mixing, respectively. The surface wind-wave mixing scheme developed by Hu and Wang (2010), which originated from the wave-induced mixing theory by Yuan et al. (1999) and Qiao et al. (2004), is employed for an improved simulation of mixing processes. More details can be found in Bai et al. (2013).

Since ice is a nonnegligible phenomenon in Lake Superior, considering its impact on currents and thermal structure evolution, the model is run with a coupled ice model based on the Los Alamos Sea Ice Model (CICE) (Hunke & Dukowicz, 1997) with the elastic–viscous–plastic rheology for the ice dynamics. More details can be found in Anderson et al. (2018) and Fujisaki-Manome and Wang (2016). Although heavy ice conditions were not observed in particular in 2010, it is preferable to enable ice coupling in a multiyear simulation to minimize discrepancies in the temperature variation over time.

The model domain covers Lake Superior with an average spatial resolution of 4.5 km (Figure 1). In the vertical direction, a 21-layer terrain-following coordinate with higher resolution placed near the surface and bottom was adopted. The minimum depth was set to 10 m to ensure global stability, that is, $\mathbf{h} + \zeta > 0$ (h is the undisturbed water depth and ζ is the free surface elevation, Wang, 1996). In this study, the leapfrog (centered differencing) scheme for time discretization was used to replace the Euler forward scheme in the internal mode and the Euler forward Runge–Kutta scheme in the external mode in the ocean momentum equations (Bai et al., 2020; Fujisaki-Manome & Wang, 2016). The reason is that the two-time step Euler forward scheme with explicit treatment of Coriolis terms has been proven inertially unstable, while the leapfrog scheme is inertially neutral stable (Wang & Ikeda, 1997a, 1997b). The model was run from 1993 to 2016, initialized in January 1992 with a uniform water temperature of 3°C and allowed to spin-up for 1 year before the simulation period began. Three-hourly atmospheric forcing with a uniform horizontal resolution of 32 km from the North American Regional Reanalysis (NARR) (Mesinger et al., 2006) is applied to the model, including surface winds, air temperature, net downward shortwave radiation at the surface, total cloud cover, and specific humidity. Since the incoming shortwave radiation can penetrate into the water column below the surface, the classification by Jerlov (1968, 1976), with the interpretation by Paulson and Simpson (1977), is applied for the specification of wave radiation. The long-wave radiation is calculated as a function of the air temperature, the model surface water temperature, and the cloud cover (Wyrtki, 1965). Latent and sensible heat fluxes are calculated by a bulk aerodynamic formulation where the transfer coefficients are calculated by considering the appropriate stability parameter (Large & Pond, 1982). The modeling results from 1993 to 2016 are produced with a time interval of 6 h.

Figure 2. Locations of the buoys (squares) and the mooring locations (blue asterisks). Contour: bathymetry (in meters). Five transects (white lines, perpendicular to the northwestern shoreline of the lake) are used for further analysis.

3. Observations

For model validation and analysis, measurements including hourly surface water temperature and wind above the lake surface are collected from the National Oceanic and Atmospheric Administration's (NOAA's) National Data Buoy Center (NDBC). The locations of the buoys and coastal sites are shown in Figure 2, where the buoy names are denoted by five-digit numbers or combinations of numbers and letters. Temperature profile measurements were collected using a combination of Seabird and RBR thermistors on moorings at three locations, denoted as Western Mooring (WM), Central Mooring (CM), and Eastern Mooring (EM), respectively (Austin, 2013; Titze & Austin, 2014). The bathymetry and five transects across the lake, which are used for further analyses, are also shown in Figure 2. The satellite-derived surface temperature data by the Great Lakes Surface Environmental Analysis (GLSEA), which are a daily, 5-day-averaged, and cloud-free surface water temperature data set derived from near real-time NOAA/AVHRR satellite temperature imagery obtained through the CoastWatch program at the NOAA Great Lakes Environmental Research Laboratory (GLERL) (Schwab et al., 1999), are adopted for comparison. GLSEA composite charts are geographically corrected and cloud-free with a spatial resolution of about 1 km. GLSEA data are validated at GLERL using in situ water temperatures from buoy measurements and have been produced daily since 1994. Detailed methodology and algorithms can be found in Schwab et al. (1999) and Schwab and Bedford (1999). Due to its algorithm and validation process, it is reasonable to use GLSEA data as quasi-observations, and it has been found to be better than the original satellite imaginary for Great Lakes studies (Plattner et al., 2006).

4. Results

4.1. Model Validation

The modeling results are validated against observations including NDBC buoy measurements and mooring data. The modeled water temperature is compared against measurements at Buoy 45023 (Figure 3), which is located on the west coast of the Keweenaw Peninsula (Figure 2). Water temperature profiles at WM are also used for comparison to examine the model's behavior vertically (Figure 4). The root-mean-square deviation (RMSD) and the mean bias (MB) are employed as a means of quantitative analysis, the definitions of which are described as follows:
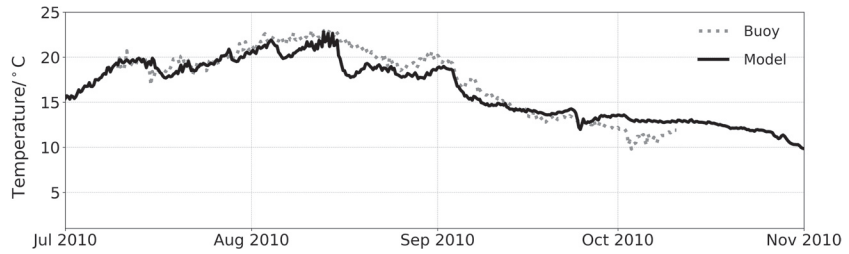
Figure 3. Water surface temperature comparison against measurements at Buoy 45023 in 2010.

$$\mathrm{RMSD} = \sqrt{\frac{\sum_{i=1}^{N} \left(\hat{x}_i - x_i \right)^2}{N}} \tag{1}$$

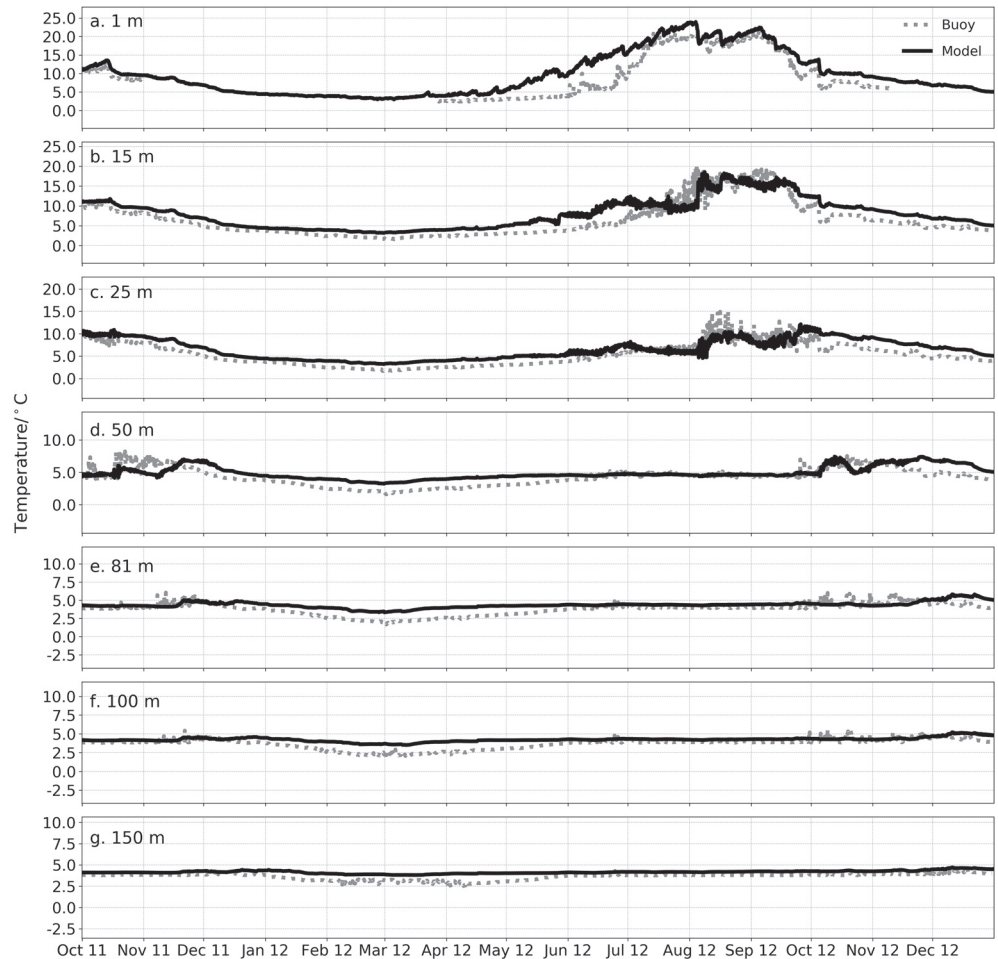$$\mathrm{MB} = \frac{\sum_{i=1}^{N} \left(\hat{x}_i - x_i \right)}{N}, \tag{2}$$

Figure 4. Water temperature profile comparison against measurements at the Western Mooring (WM) during 2011 and 2012.

Table 1
Root-Mean-Square Deviation (RMSD) and Mean Bias (MB) at the Western Mooring (WM)

Depth (m)	RMSD (°C)	MB (°C)
1	2.74	2.31
15	1.57	1.48
25	1.44	1.38
50	1.32	0.79
81	1.03	0.82
100	0.98	0.81
150	0.72	0.64

where $\hat{x}_i$ and x_i $(i = 1,2,\ldots,N)$ are the modeled and measured time series, respectively, N is the total number of the sample, and the over bars mean the averaged value of the time series.

It can be seen that the overall performance of the model at Buoy 45023 in coastal waters is acceptable: the RMSD and MB values are 1.29°C and −1.27°C, respectively. A slight underprediction is found, as indicated by the MB value.

To examine the model's ability to predict thermal stratification, the water temperature profile comparison to the WM measurements from October 2011 to December 2012 is shown in Figure 4. Water temperature comparisons at 1, 15, 25, 50, 81, 100, and 150 m depth are presented in sequence. The RMSD and MB values at each depth are shown in Table 1. The largest discrepancy is observed 1 m below the surface, where the onset of temperature rise is predicted approximately 1 month earlier by the model.
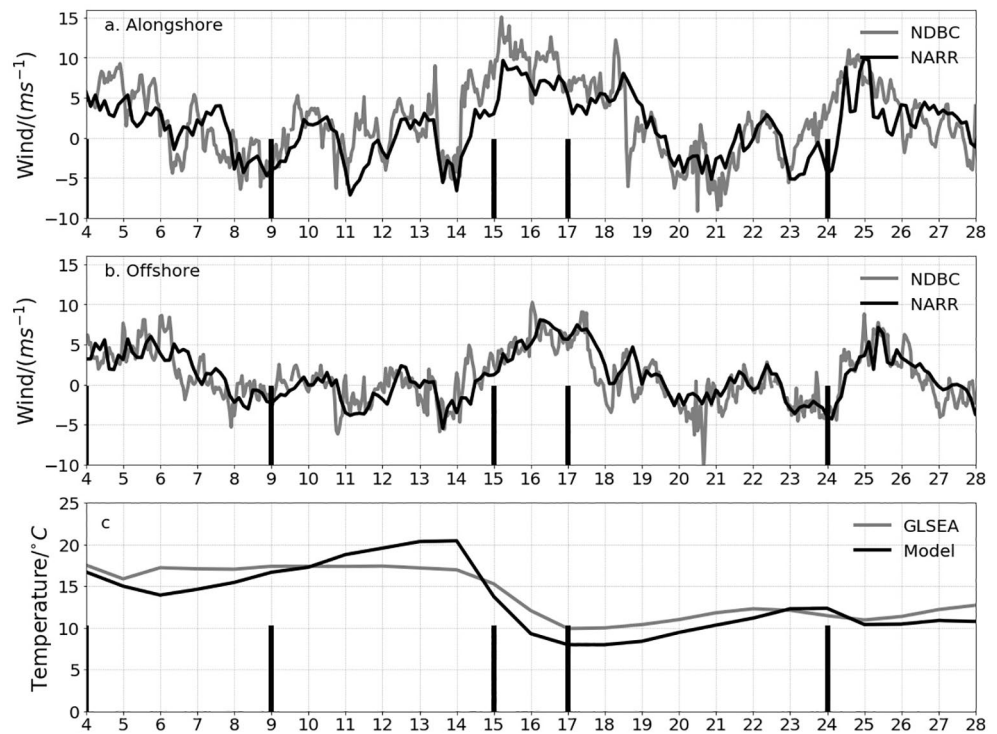
Referring to Table 1, the RMSD values vary between 0.72°C and 2.74°C, and the MB ranges from 0.64°C to 2.31°C, indicating a warm bias of the model through the whole water column. Overall, model skill is consistent with other 3-D modeling studies in Lake Superior and other lakes, for example, it is comparable to (slightly better than) Bennington et al. (2010)'s results with RMSD being 3.4°C. Moreover, the majority of temperature fluctuations during summer and early fall and the monotonic trend in winter and spring at each layer are very well resolved. Overall, the model predicts thermal stratification reasonably well. The water temperature below 25 m is much less influenced by meteorological conditions and stays almost constant the whole year around, especially at depths below 50 m.

In summary, despite some discrepancies, the performance of the model at various locations in the lake with various water depths and in different seasons is reasonable, giving confidence in our analysis based on the modeling results. Model validation for currents can be found in Bai et al. (2013).

Since the temporal and spatial resolution and quality of the wind forcing have been regarded as one of the most important factors leading to a reliable prediction of the temperature field (Beletsky et al., 1997, 2013; Chen et al., 2004), the wind measured at DISW3 (which is located between transects 1 and 2) and the corresponding wind forcing from NARR used in the model are compared in Figure 5. The time series comparison at this station is selected as a sample to see the quality of the NARR wind and its impact on the computed temperature field in the selected area (Figure 1). The alongshore (toward NE being positive) and offshore wind components are compared in Figures 5a and 5b, respectively, the RMSD of which is 3.53 and 2.23 m s^{-1}, respectively. The RMSD of averaged temperature in the selected upwelling zone (see Figure 1 for the location) between the model and the GLSEA chart shown in Figure 5c is 1.84°C, and the MB is −0.71°C. This result demonstrates that the wind quality of NARR is acceptable to use in a 3-D ocean model to resolve upwelling events and that the model results forced by NARR wind are reasonable, which reassures the reliability of applying the modeled results in detailed upwelling analyses. Referring to the alongshore wind, which has significant implications on upwelling events, 5 days are selected for investigations: August 4 when onset of upwelling-favorable wind was observed; August 9 when alongshore wind almost ceased; August 15 when alongshore wind started growing again after a relatively calm period; August 17 when the peak magnitude just passed; and August 24 at the end of another relatively long period of calm conditions.
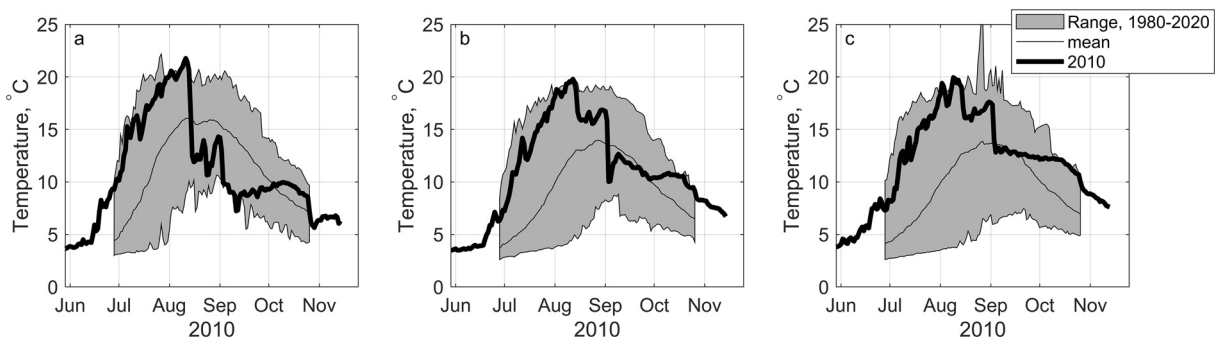
4.2. Temperature

Upwelling events are good examples of synoptic scale processes in the Great Lakes. However, due to the complex nature of mixing and advection processes involved, it is difficult for numerical models to produce accurate predictions. Observations show that prior to the upwelling event in question 2010 was an exceptionally warm year in Lake Superior compared to the long-term mean (Figure 6). The observed temperatures at the three moorings are 5°C–13°C higher than the average temperature during 1980–2020. The observed data also show a large temperature drop at the three moorings in mid-August 2010—especially dramatic at WM in the western basin of the lake—suggesting the occurrence of an upwelling event. Data from GLSEA confirm an upwelling event off the northwestern shore of Lake Superior, and it is reproduced by our model.
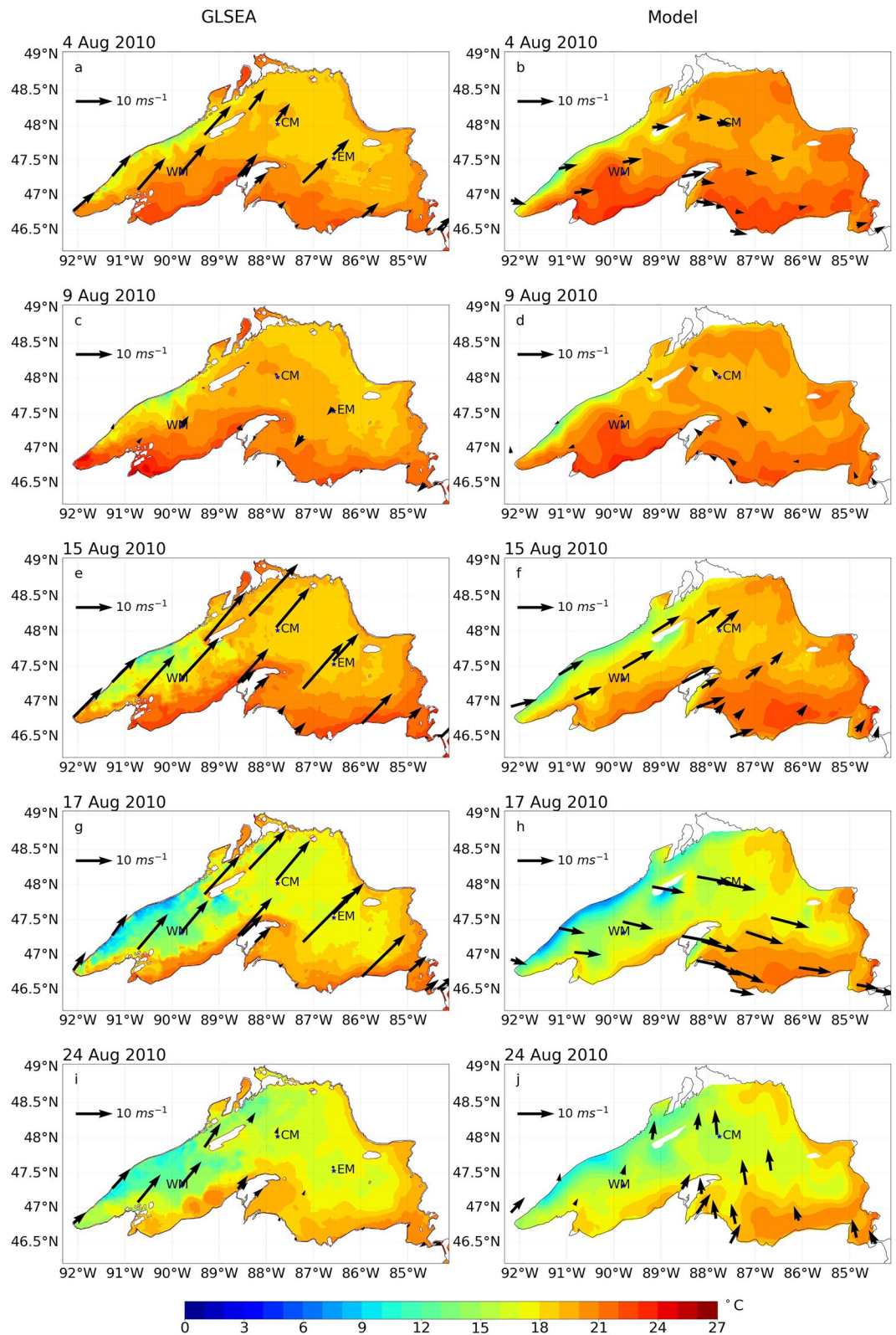
Figure 5. (a) The alongshore wind component at DISW3, (b) the offshore wind component at DISW3, and (c) zone-averaged surface water temperature from August 4 to August 28, 2010. Heavy vertical bars mark the location of selected dates.

Figure 7 shows the evolution of the surface water temperature during the 21 days of this upwelling event, with the surface wind superimposed on the temperature map on the selected days. The daily GLSEA composite charts are shown in the left column, superimposed with daily-averaged lake surface wind measured at NDBC buoys. The 5-day-averaged modeling results with daily-averaged NARR wind are shown in the right column. It is noticeable that the NARR wind in Figure 7 is averaged from a 3-hourly climate data set while the wind observations from NDBC are averaged from hourly observations from buoys only. Discrepancies, such as slightly higher temperature in the eastern basin of the lake and lower temperature on the south shore of Isle Royale, are also found. For example, on August 17, the daily-averaged northwesterly NARR wind resulted in relatively smaller areas being influenced by the upwelling, while in the GLSEA chart, a larger area was influenced by the upwelling, corresponding to a stronger alongshore wind. Nevertheless, the modeling results match reasonably well the GLSEA data. The modeled temperature distribution is quantitatively similar to the GLSEA chart. The overall temperature patterns across the lake, the
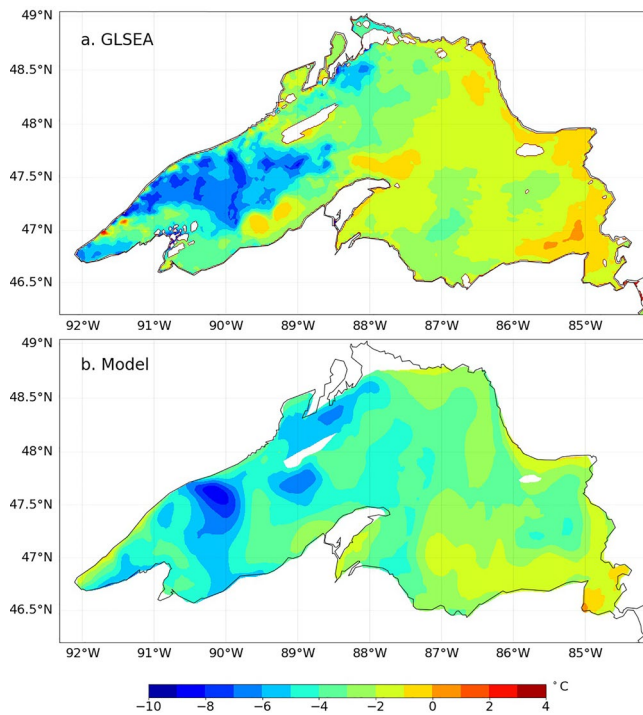

Figure 6. Daily-averaged surface water temperature at three sites on Lake Superior. Shaded region is observed range, 1980–2020; thin line is mean over the same range; thick line is 2010. (a) Buoy 45006, Western Superior; (b) Buoy 45001, Central Superior; and (c) Buoy 45004, Eastern Superior.

Figure 7. Water surface temperature distribution on five selected days between August 4 and August 24 in 2010 from GLSEA charts (left column) and the model (right column). Black arrows in the left column: wind observation from NDBC; black arrows in the right column: wind forcing from NARR. GLSEA, Great Lakes Surface Environmental Analysis; NDBC, National Data Buoy Center; NARR, North American Regional Reanalysis.

Figure 8. Water surface temperature change between August 4 and August 24, 2010. (a) GLSEA and (b) Model. GLSEA, Great Lakes Surface Environmental Analysis.

temperature magnitudes, the areas of dramatic temperature variations, and the location of upwelling are all resolved by the model.

A southwesterly wind, which was parallel to the northwest shore, prevailed over the lake (with an exception on August 9, 2010, when the wind almost ceased). As shown in previous studies (Niebauer et al., 1977), this is one of the prerequisites for the occurrence of upwelling. The southwesterly wind at a magnitude of 10–20 m s^{-1} was observed on August 4 when the first signs of the coastal upwelling started emerging. The most impacted area during this upwelling event is the northwestern shore between Duluth and Thunder Bay. The upwelling area, characterized by a lower temperature nearshore, first appeared on the coast between Two Harbors and Thunder Bay in early August (Figures 7a and 7c). It then extended to Duluth in mid-August and reached its peak (Figures 7e and 7g), followed by relaxation in late August (Figure 7i). Weaker alongshore wind component in NARR led to a somewhat weaker upwelling in Duluth Basin in the model (Figures 7h and 7j vs. Figures 7g and 7i).

As mentioned before, on August 9, the wind slowed down (Figure 7c) and the upwelling influenced area remained stable without apparent expansion. Starting in mid-August, during which the wind speed reached over 30 m s^{-1}, a larger upwelling zone that extended to Duluth was formed. A small upwelling zone on the southwest shore of Isle Royale was also observed during this time (Figures 7e and 7g). The water temperature in the Duluth Basin and Apostle Basin decreased by over 10°C toward late August (Figure 8) while the temperature drop in Keweenaw Basin, which was only slightly influenced by this event, was only approximately 5°C over the 21 days. This development process is well captured by the model (right col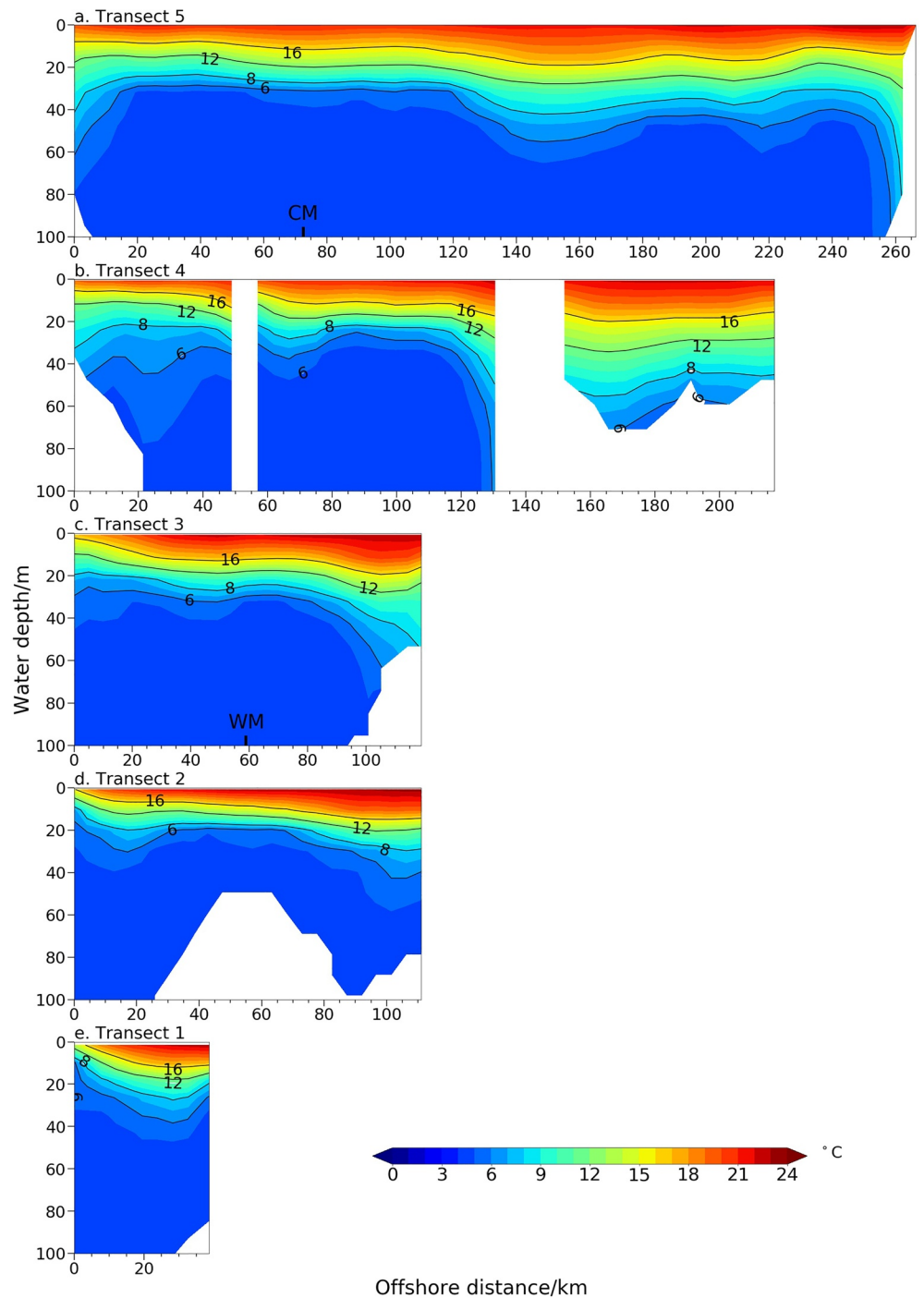umn of Figure 7). However, the upwelling influenced area on the south shore of Isle Royale was overestimated in mid-August compared to the GLSEA chart, which shows that only a small area on the south shore of Isle Royale was impacted (Figures 7e and 7g). Discrepancies between the NARR wind used in the model and wind observations from NDBC, especially the errors in wind direction, play a role in this overestimation.

The surface temperature change from August 4 to August 24, 2010, is shown in Figure 8, where the modeled results (lower panel) are roughly consistent with the GLSEA chart (top panel) in most areas of the lake. The temperature drop in the western basin of the lake, which is the area most impacted by the upwelling event, ranges within −2°C to −10°C, whereas in the eastern basin, it is typically −1°C to −5°C.

To further study the upwelling event, temperature evolution is examined at five selected transects across the lake (shown in Figure 2). Transects 1–3 are between Two Harbors and Thunder Bay, where coastal upwelling happens most frequently. The starting point of transect 4 is located off the northeast of Thunder Bay and intersects Isle Royale and the Keweenaw Peninsula. Transect 5 is the northernmost, extending to the eastern lake, across the Keweenaw Basin, and intersecting the two areas with the largest bathymetry gradient. The direction of all transects is toward the southeast, that is, offshore, starting from the northwest shore. As seen from the surface temperature field (Figures 7 and 8), transects 1–3 are in the area most impacted by the upwelling event.
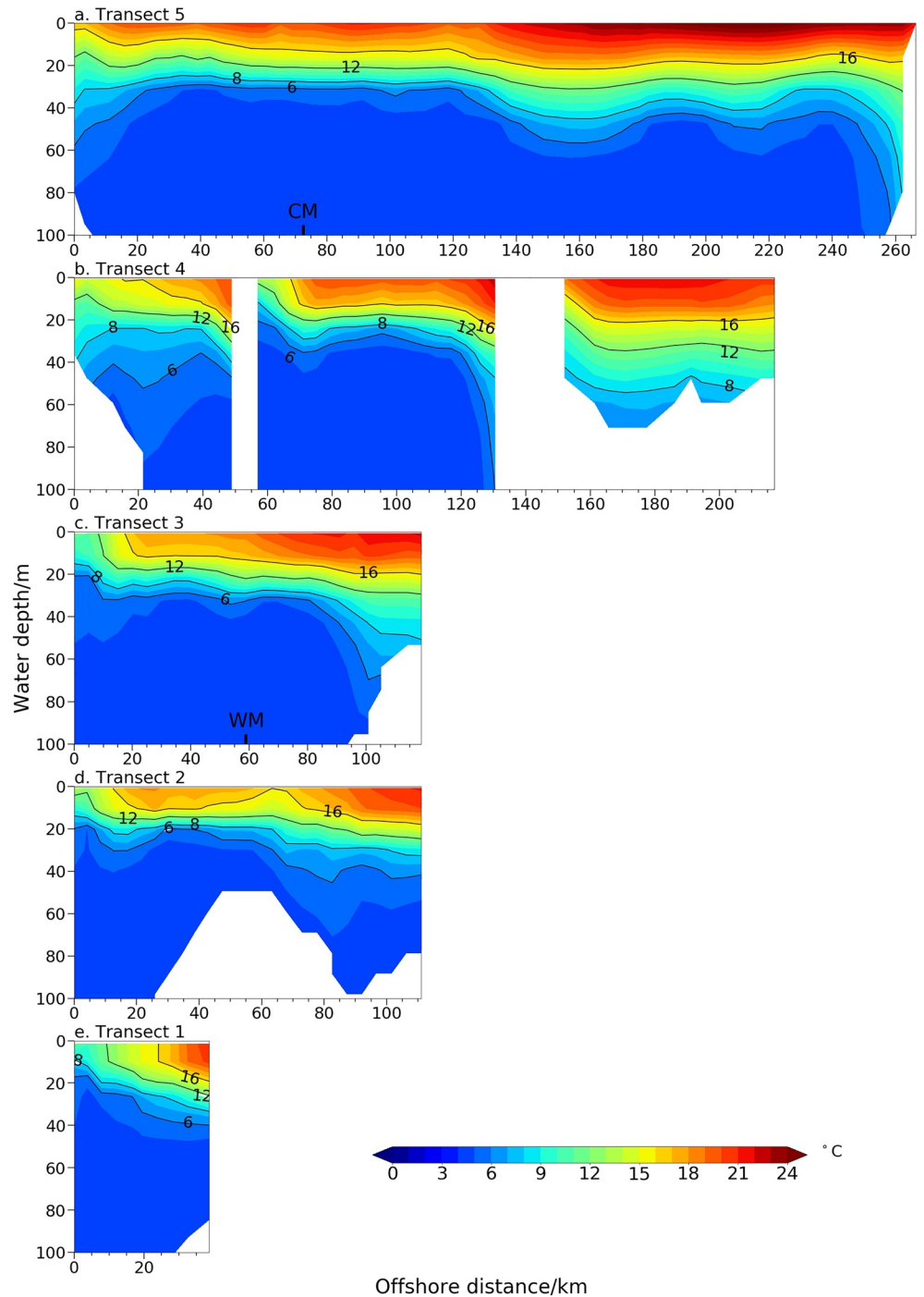
Temperature distribution in the vertical at the selected transects on August 4, August 15, and August 17 is shown in Figures 9, 10, and 11, respectively. In these transect views, the strongly stratified status, the tilt and surfacing of the thermocline, and offshore displacement of upwelling front are all well modeled.

Upwelling started emerging on August 4 (Figure 9), with the onset of upwelling-favorable alongshore wind, and reached its peak on August 15–17 (Figures 10 and 11). On August 4, the modeled upper mixed layer (epilimnion) was quite shallow, usually less than 10 m at the selected transects. The thermocline zone (metalimnion) was located between 10 and 50 m. The isotherms were nearly horizontal at each transect, except in the upwelling areas at transect 1 and transect 2 where the surfacing of thermocline started
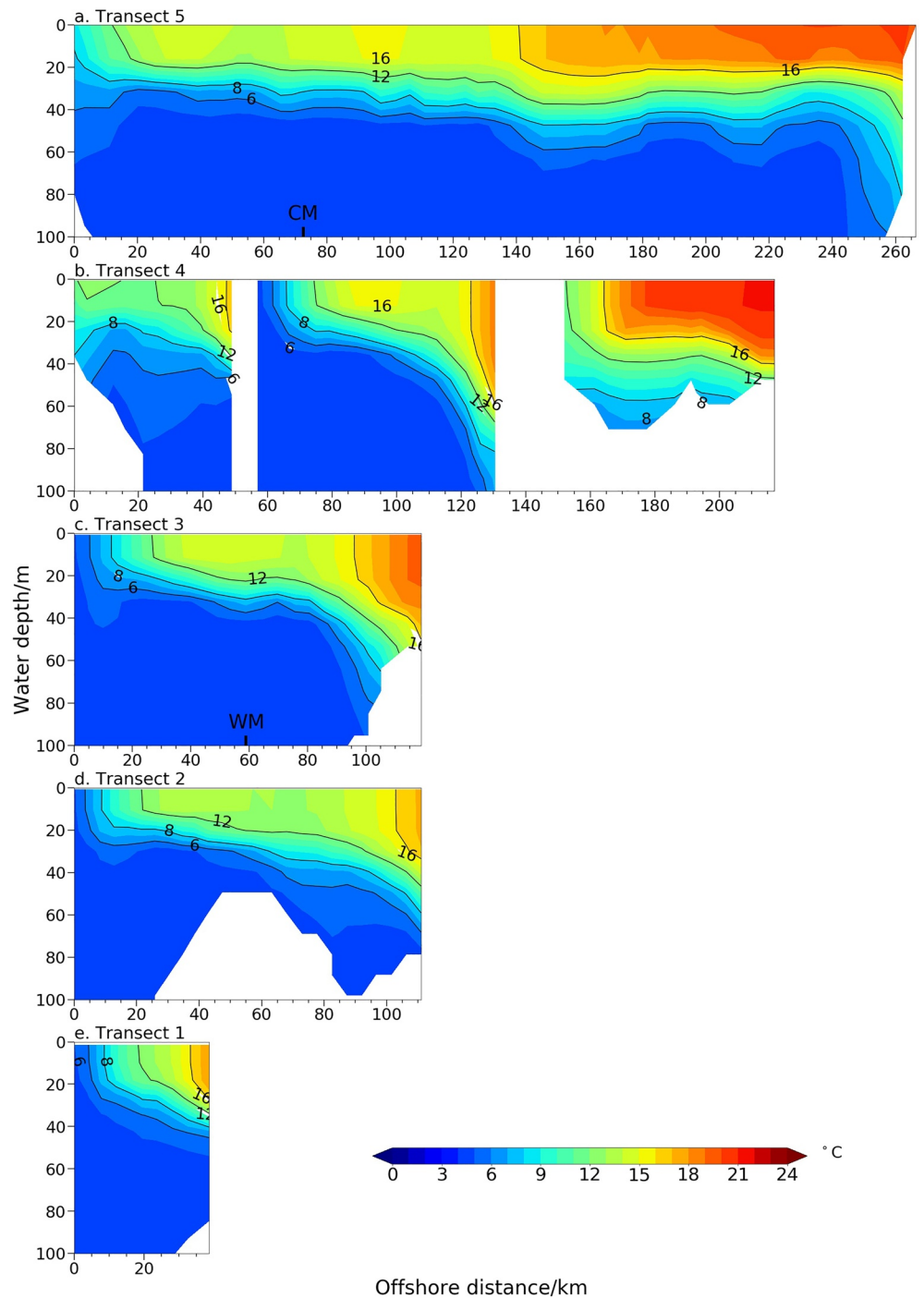
Figure 9. Temperature distribution at the selected transects on August 4, 2010.

appearing (Figure 9). On August 15, coastal upwelling on the northwestern shore was strong enough to advect the thermocline 20–30 km offshore at transects 1–3 (Figure 10) and low-temperature water from below 50 m upwelled to the surface. Meanwhile, downwelling on the southeastern coast was signaled by mild downward tilt of isotherms. A "full" upwelling, where the thermocline intersects the free surface (Csanady, 1977), was rather prominent starting August 15 across transects 1–4 (Figure 10). At this point, the isotherms at transects 1–4 were remarkably distorted by the upwelling. The warm water initially in the epilimnion was replaced by cold water below 16°C at transects 1–4, with an impacted offshore distance as

Figure 10. Temperature distribution at the selected transects on August 15, 2010.

far as 25 km at transects 1–3. At transect 4, which is partitioned by Isle Royale and the Keweenaw Peninsula, the initial epilimnion to the north was completely overturned by the upwelling. Downwelling on the southeastern coast at these transects was also more pronounced than 2 days later (Figure 11). A significant temperature decline took place in the Royale Basin, even at transect 5, which runs across the Royale Basin and the Keweenaw Basin, accompanied by a slight distortion of the isotherms in the hypolimnion on the southeastern coast. On August 17, the thermocline further continued the distortion, especially in the downwelling areas, and the significant temperature drop in the top 20 m was even more prominent (Figure 11).
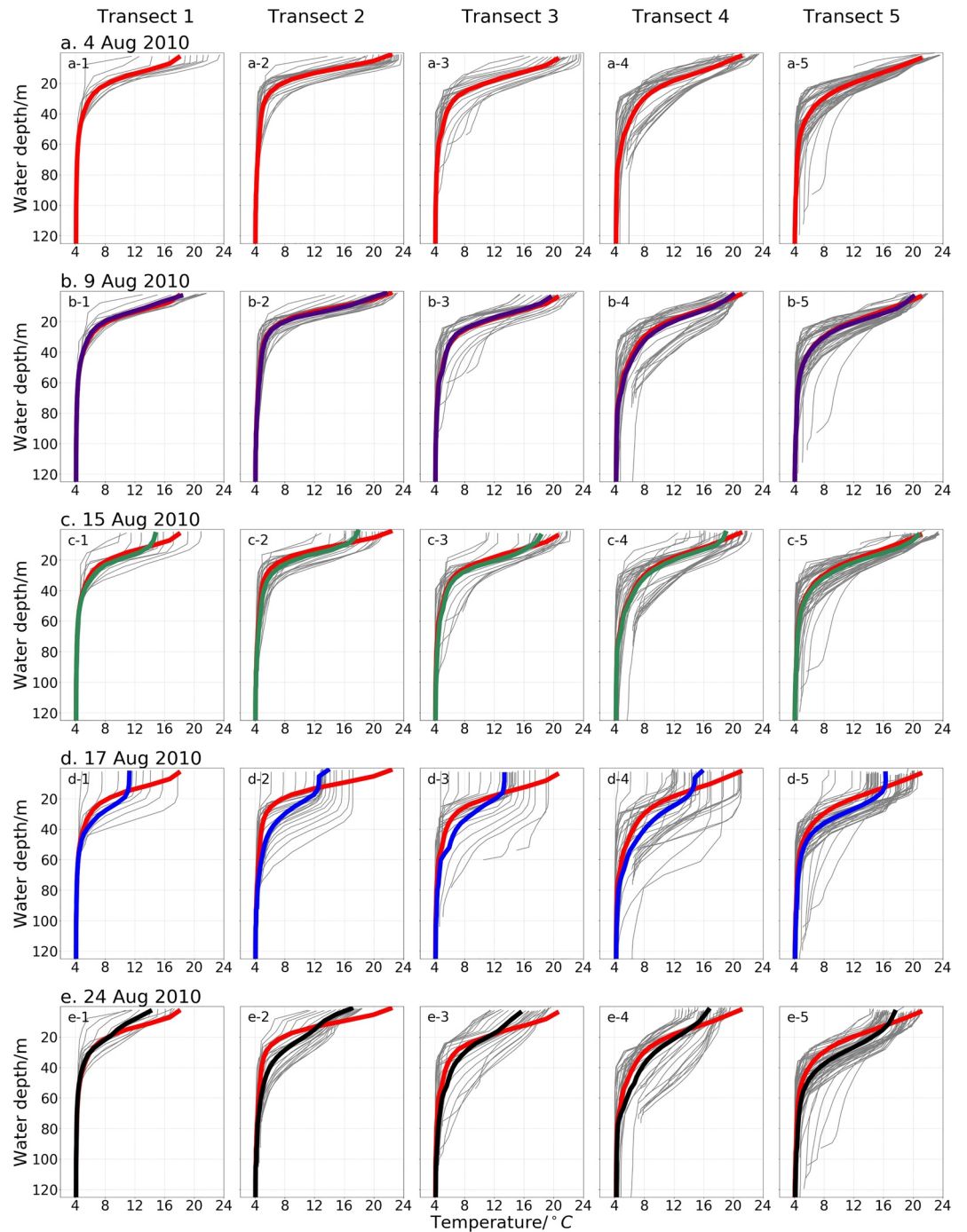
Figure 11. Temperature distribution at the selected transects on August 17, 2010.

4.3. Heat Content

Figure 12 shows the temperature profile at the five transects during the upwelling development. The mean value in each subfigure is shown by the thick colored lines, and the initial mean profile (red line) on August 4, 2010, at each transect is superimposed on the following days to see the profile evolvement. It is shown that at the beginning of the upwelling event, the thermocline was confined to the upper 40–60 m, below which was the hypolimnion where the water temperature was approximately 4°C. The mean thermocline depth is deeper at transects 4 and 5, since both are across the Royale Basin and the Keweenaw Basin and

Figure 12. Temperature profiles at the five selected transects on five selected days in August 2010. (The thin gray lines are produced from the grid points at each transect, and the heavy colored lines are the mean value in each plot.).

therefore have more diverse temperature profiles. The epilimnion was very shallow (also shown in Figure 9) and occupied only the top 5–10 m of the lake. As the upwelling developed, low-temperature water from the bottom layers upwelled and mixed with the water in epilimnion and metalimnion, resulting in the sinking and expansion of the upper mixed layer and the thermocline zone. This can be attributed to the wind-induced mixing offshore. On August 15, when the upwelling became rather prominent, the water temperature in the upper layers was 2°C–4°C lower than the initial value at the south 4 transects, whereas transect 5 was hardly influenced. On August 17, when the most significant change in the mean thermocline shape and

location occurred, the surface temperature drop was as large as 10°C, as shown by the distance between the red and blue line (Figure 12d). The postpeak relaxation of the thermocline was modeled on August 24 (Figure 12e).

The heat content h_c is calculated by integrating the temperature over depths, that is, $h_c = \rho c_p \int T\,dz$, where ρ is the water density (1,000 kg m^{-3}), c_p is the specific heat, T is the water temperature (in °C), and z is the water depth. In Figure 12, the area between two points of concern on the thermocline projected perpendicularly to the horizontal axis roughly demonstrates the heat content divided by ρc_p. Thus, it is evident in Figure 12 that, as of August 17, the mean heat content at transect 1 is less than its initial value on August 4. This suggests the occurrence of advective/diffusive heat flux across this transect, since the total heat content at a transect does not change due to upwelling. Whereas the heat content at other transects is approximately unchanged from their initial values, indicating strong mixing instead. It suggests that the heat content in shallow areas is impacted more directly than in deep waters. Note that not all the locations in the same transect were impacted by upwelling, and the individual profiles to the right of the mean profile were those located in the weakly impacted areas. By August 24, the upwelling had vanished, leaving a postevent low-temperature and the mean temperature profiles relaxed slightly back toward the initial position.
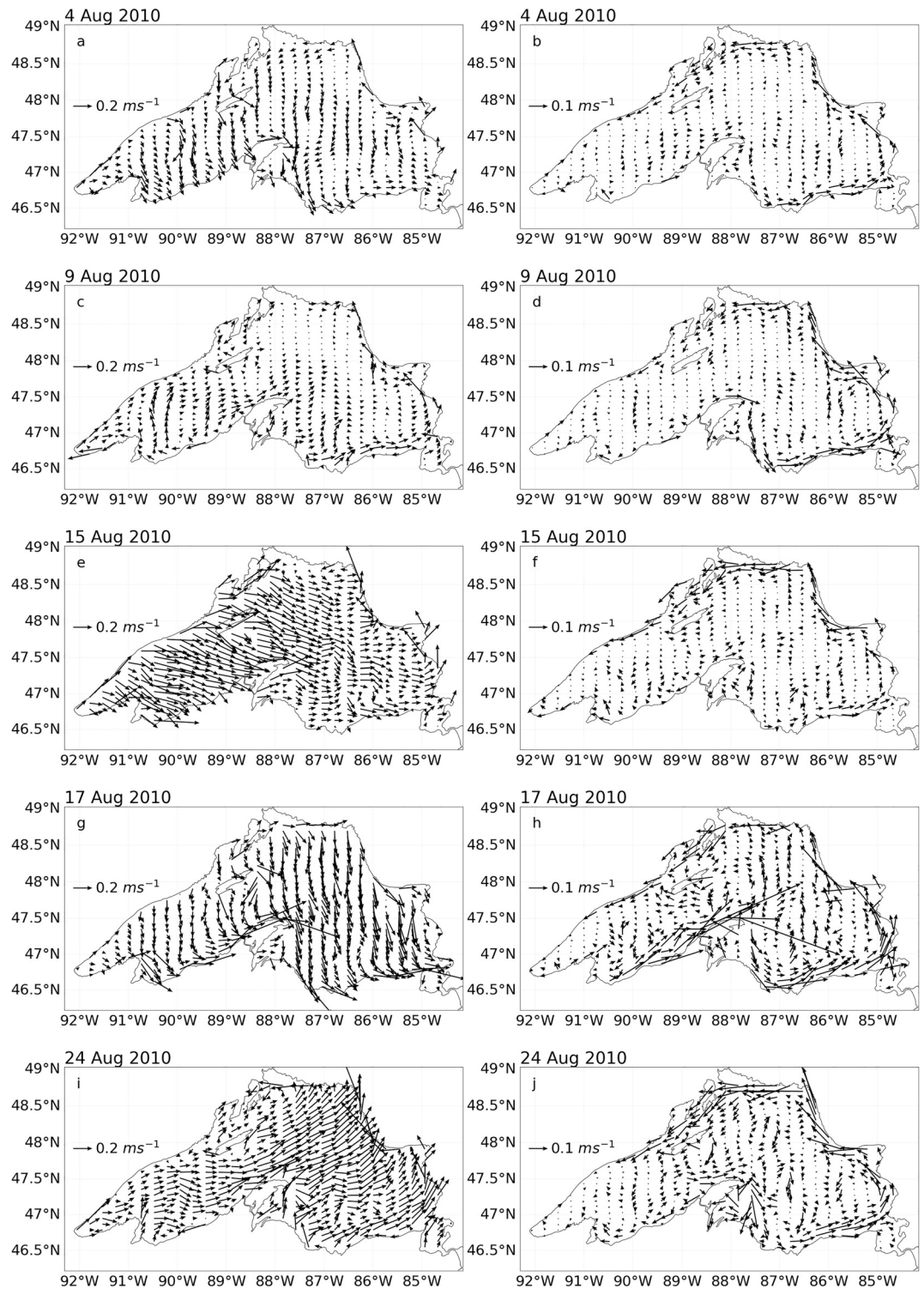
4.4. Currents

Figure 13 shows the daily-averaged current fields, after low-pass filtering to remove the near-inertial oscillations, on the five chosen days. Since the inertial period ranges from 16 to 16.5 h in Lake Superior, depending on the local latitude (Austin, 2013), a cutoff of 17 h is adopted in the filter. A particularly strong current was modeled on the west side of the Keweenaw Peninsula in mid-August, driven by strong shore-parallel wind with a peak current speed over 0.7 m s^{-1}. Similar current speeds were also reported by Niebauer et al. (1977). The surface current in the upwelling area, usually smaller than 0.1 m s^{-1}, was smaller than the rest of the lake. On August 4, the surface currents were generally offshore to the south in the Apostle, Royale, and Keweenaw Basins and converged toward the Keweenaw Peninsula (Figure 13a). Surface currents were the smallest among the five selected days on August 9, since wind almost ceased at that time (Figure 13c). On August 15, surface currents were generally eastward, with a slight cyclonic bend (Figure 13e). Due to the strong winds in mid-August, the current flowed from the north shore to the south shore of the lake on August 17 (Figure 13g), resulting in a dramatic water temperature drop. A cyclonic pattern (Figure 13g) or a generally eastward current (Figure 13i) was modeled later when the wind gradually slowed down. Only on August 9, when the wind temporarily ceased, was a northward onshore flow modeled. Otherwise, the currents in the Duluth Basin and the Apostle Basin were flowing either eastward or southward. Shown in the right column of Figure 13, the currents at a water depth of 30 m were substantially weaker, except for the Keweenaw Peninsula area and along the perimeter of the Keweenaw Basin, where the current speed was approximately 0.1 m s^{-1} most of the time.
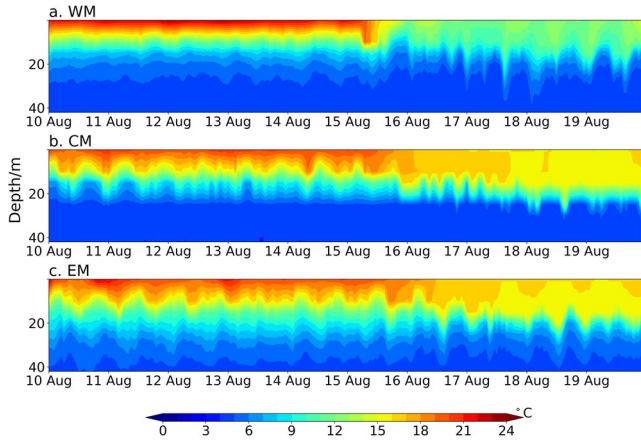
5. Discussions

5.1. Heat Content and Advection Process During Upwelling

The time-evolving temperature profile measured at the WM, CM, and EM is shown in Figure 14, and the corresponding modeled results are shown in Figure 15. Since WM and CM are close to transects 5 and 3, respectively, their distance off the northwestern coast is also marked in the transect views in Figures 9–11. A sudden temperature drop in the upper 10 m was first observed at WM on August 15, 2010, due to the arrival of the upwelling front (also Figure 10), after which the surface temperature remained low until August 20. A day later, the temperature dropped at CM as well, but the temperature decline was less than that at WM. Another 12 h later, a similar temperature drop was observed at EM. Referring to results in the preceding sections, the temperature drop at WM is due to the arrival of the upwelling front (also Figures 7, 10, and 11), while that at CM and EM is the result of the vertical mixing due to the strong wind. The temperature evolution pattern is well reproduced by the model (Figure 15), but the time lag between EM and CM was larger than in observations.

Figure 13. Surface current (left column) and current at 30 m (right column) on five selected days from August 4 to August 24, 2010.

Figure 14. Temperature profile measurements at the three mooring locations from August 10 to August 20, 2010.

Figure 15. Modeled temperature profile at the three mooring locations from August 10 to August 20, 2010.

The heat content calculated from measurements at the three moorings is shown in Figure 16 and can be used as indicator of upwelling extent in the lake. A significant drop in the heat content was seen on August 15 at WM, suggesting strong advection due to the arrival of the upwelling front. This was also supported by the current field, where advection of cold water from the west (Figure 13e) was modeled. On the other hand, heat content was gradually increasing at CM indicating the advection of warm water, which was confirmed in the current field (advection of warmer waters from the north and east) as seen in Figures 13g and 13h. The easternmost mooring (EM) was not impacted by the upwelling event, exhibiting only weak fluctuations of heat content. Figure 17 shows the simulated heat content by the coupled model, with the above features captured well, although there are discrepancies in the magnitude.

5.2. Upwelling Front Displacement

When a wind impulse is strong enough to cause the surfacing of the thermocline, as usually seen in upwelling events, one subsequent question is how far it can move from the shoreline. Knowledge of offshore thermocline displacement is important for a variety of processes from physics (e.g., mixing is enhanced in unstratified conditions in full upwelling area) to chemistry and ecology (e.g., bottom layer is interacting directly with atmosphere impacting gas exchange). The offshore displacement itself is also a good indicator to measure the upwelling strength, since it is closely related to the wind stress. Csanady (1977, 1982) applied the potential vorticity equation to a two-layer model (above and below the thermocline) to study the offshore thermocline displacement induced by alongshore wind. For simplicity, the vorticity equation was applied to two layers, respectively, with an assumption of an evenly distributed wind stress imposed only as a short burst over the top layer, therefore zero curl of the wind stress is ensured (Csanady, 1982). Csanady (1977) demonstrated the very limited effect of this assumption on the solution. Csanady (1977, 1982) provided a simple analytical solution:
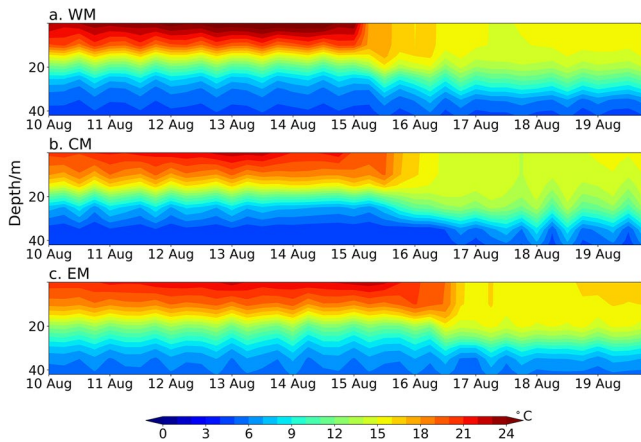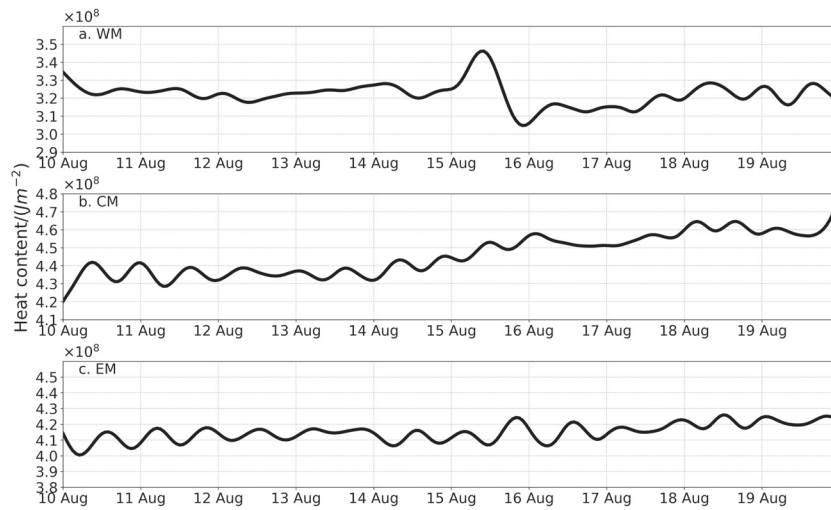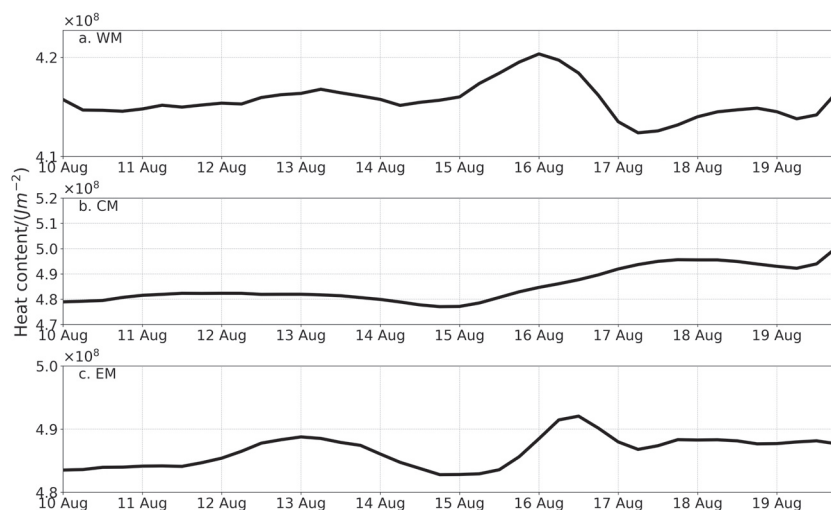
$$x_0 = \frac{I}{fh_t}\frac{h_b}{h_t + h_b} + R_2, \tag{3}$$

where x_0 is the offshore displacement of the thermocline, f is the Coriolis parameter, h_t and h_b are the depth of the top and bottom layer, respectively, $I = \int \frac{\tau_y}{\rho}\,dt$ is the time-integral of the alongshore wind impulse, and R_2 is the internal radius of deformation described by

$$R_2 = f^{-1}\left(\frac{\epsilon g h_t h_b}{h_t + h_b}\right)^{1/2}, \quad x \leq x_0, \tag{4}$$

in which τ_y is the alongshore wind stress, t is time, $\epsilon = \dfrac{\rho' - \rho}{\rho'}$, ρ and ρ' is top and bottom layer water density, respectively, and g is the gravitational acceleration.

Taking transect 3 as an example, based on the thermal structures on August 4, August 15, and August 17, 2010 (see Figures 9, 10, and 11), we take the isotherm of 12°C as the interface between the top and bottom layer, which is a reasonable application of Csanady (1977)'s theory where the midthermocline location is taken as the interface. We have the total water depth as the average depth within 20 km from the coast as done by Csanady (1977), which is 156.29 m for transect 3, and $g = 9.8\,\mathrm{m\,s^{-2}}$, $\rho' = 999.50\,\mathrm{kg\,m^{-3}}$, and $\rho = 998.70\,\mathrm{kg\,m^{-3}}$ according to the equation of state, and $f = 1.072 \times 10^{-4}\,\mathrm{s^{-1}}$. We have $h_t = 19\,\mathrm{m}$, $I = -28.58\,\mathrm{m^2\,s^{-1}}$, and
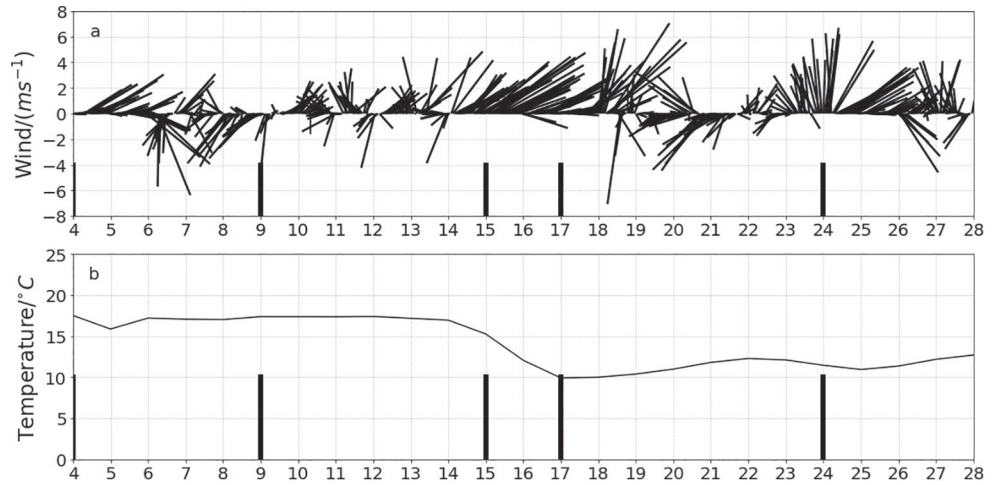
Figure 16. The observed heat content calculated at the three mooring locations from August 10 to August 20, 2010: (a) Western Mooring, (b) Central Mooring, and (c) Eastern Mooring.

R_2 = 3.39 km on August 15, and h_t = 16 m, I = −51.76 m^2 s^{-1}, and R_2 = 3.14 km on August 17, 2010. Note that the wind impulse is integrated from August 2 when surfacing tendency of the isotherm being 12°C was not as prominent as of August 4 (Figure 9). Applying them to the theoretical formula by Csanady (1977, 1982), the calculated offshore displacement of the thermocline on August 15 and August 17 is 9 and 24 km, respectively. On August 15, the modeled offshore displacement is 9 km, remarkably close to the calculated value. However, on August 17, the modeled offshore displacement is approximately 25 km, roughly 1 km farther than the calculated value. Although many assumptions are implicated in the theory by Csanady (1977), its purpose to estimate the offshore displacement of the upwelling front is well served as examined by a more advanced numerical model. The simple relationship between the thermocline offshore displacement and the wind stress derived by Csanady (1977, 1982) is proven to be an efficient tool for estimation, especially when limited information is available for complicated calculations.

Figure 17. The modeled heat content at the three mooring locations from August 10 to August 20, 2010.
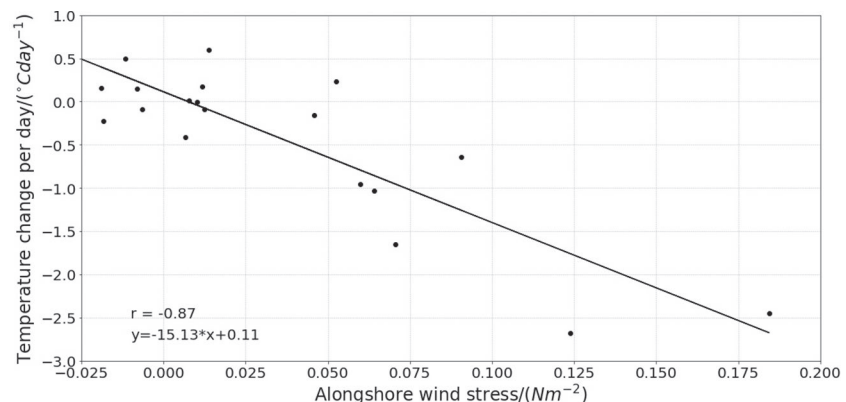
Figure 18. (a) Wind velocities at DISW3 and (b) zone-averaged surface water temperature from the GLSEA charts from August 4 to August 28, 2010. GLSEA, Great Lakes Surface Environmental Analysis.

5.3. Alongshore Wind and Temperature Change

The temperature decrease in the coastal zone is a signature feature of upwelling. Its association with alongshore wind u_a is studied using time series of wind measured at DISW3 (converted to wind stress using $\tau_y = C_d \rho_a |u_a| u_a$, where C_d is the drag coefficient, ρ_a is the air density) and the zone-averaged water temperature from the GLSEA charts (Figure 18). The drag coefficient is specified according to the Large and Pond (1981) approach. The area selected for temperature analysis is shown in Figure 1. The dramatic temperature drop from August 15 to August 17, 2010 in Figure 18b is concurrent with persistent alongshore wind (i.e., southwesterly wind) at DISW3 (Figure 18a). Surface temperature change derived from daily GLSEA data during the period of upwelling (August 4–28) versus daily wind stress is shown in Figure 19. The correlation coefficient r is as significant as −0.87, indicating a strong impact of the alongshore wind on the resulting temperature decrease. To explore this relationship further, a simple heat balance model was developed for the offshore transect (Figure 20).

Alongshore wind stress drives a predictable cross-shelf transport in a surface Ekman layer, which is compensated by a deep return flow. Assuming that alongshore temperature gradients are weak, it does not drive any appreciable change in the heat content of the shelf. A simple heat balance can be derived:

$$A\frac{d\overline{T}}{dt} = -U\left(T + \Delta T\right) + UT, \tag{5}$$

Figure 19. Upwelling-favorable alongshore wind stress at DISW3 versus time derivative of the zone-averaged surface water temperature from August 4 to August 28, 2010.
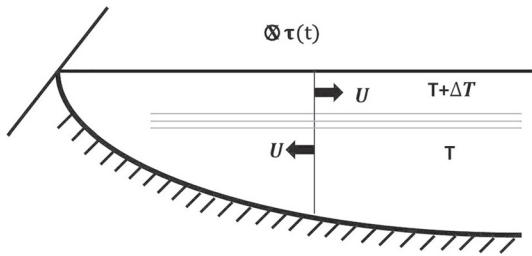
Figure 20. Schematic diagram of cross-shelf transport model.

where t is time, $\overline{T}$ is the temperature averaged over an area, A is the cross-sectional area (depth multiplied by offshore distance—we assume that alongshore variations are small and the problem reduces to a 2-D slice), U is the transport in the upper layer, which by continuity must be balanced by a reciprocating onshore flow at depth of the same magnitude, T is the temperature at depth and ΔT is the temperature difference between the surface and the bottom layer. Note that this ignores surface heat fluxes and alongshore variability.

The transport in a steady Ekman layer can be expressed as

$$U = \frac{\tau_y}{\rho f}. \tag{6}$$

Combining Equations 5 and 6 yields

$$\frac{d\overline{T}}{dt} = -\frac{\Delta T}{\rho f A}\tau_y, \tag{7}$$

indicating that the temperature change rate in an area is a function of the alongshore wind stress. The fraction at the r.h.s. of this equation is the slope of the line in Figure 19. Using data presented in Figures 9, 10, and 11, the temperature difference at transects 2 and 3, which intersect the selected upwelling zone, is 12°C–16°C. Taking $\Delta T = 14$ K, $\rho = 1.0 \times 10^3$ kg m^{-3}, $f = 1.0 \times 10^{-4}$ s^{-1}, the mean water depth = 100 m, and the offshore distance being 1.5×10^4 m, this fraction, $-\frac{\Delta T}{\rho f A}$ equals to $-9.3 \times 10^{-5} \frac{\text{K/s}}{\text{N/m}^2}$ or $-8 \frac{\text{K/day}}{\text{N/m}^2}$.

The slope of the regression line in Figure 19 is $-15 \frac{\text{K/day}}{\text{N/m}^2}$, of a similar magnitude to the fraction derived by Equation 7 but somewhat larger. While a simple linear heat balance model was able to explain most of time rate of change in temperature measurements, this faster time rate of temperature change in observations is likely an indication of processes omitted in the simple model, such as surface heat fluxes and alongshore variability. In addition, the offshore wind component which was quite substantial during upwelling (Figure 5) can also contribute to coastal upwelling development (Csanady, 1977) thus enhancing the temperature decrease in the coastal zone.

6. Conclusions

A strong upwelling during summer 2010 in Lake Superior was investigated using a 3-D coupled ice–ocean model and observations. The modeled temperature was compared to the moored and satellite temperature measurements. Based on the investigation above, the following conclusions may be drawn:

(1) A strong upwelling during August 15–24, 2010, which reached a peak on August 17 was reproduced by the model. A 4-day long strong, persistent alongshore wind was the major driving force of this event. During the upwelling event, the modeled offshore flow in a surface Ekman layer was driven by the alongshore wind, while the compensation flow was mainly the subsurface onshore flow and the southwestward coastal current.

(2) A cooling of as much as 10°C observed along the northwestern shore was captured by the model. A linear correlation between the surface water temperature change and the alongshore wind stress was −0.87. A simple linear heat balance model was able to explain most of time rate of change in temperature measurements.

(3) The heat content at the WM calculated from the measurements and the model shows a significant drop in mid-August, indicating the impact of upwelling while the CMs and EMs did not exhibit such decrease in heat content and were not as strongly impacted by upwelling.

(4) The simulated offshore displacement of the thermocline (upwelling front) was about 9 km on August 15 and 25 km on August 17, while the estimation using the Csanady's theory is 9 and 24 km,

respectively, indicating that, simple analytical model was able to capture the dynamics of the upwelling front movement offshore.

Data Availability Statement

For data access, the mooring observations are available at https://doi.org/10.13020/YZ65-ZC05. Surface water temperature data can be accessed at ndbc.noaa.gov. Model output is available at the NOAA National Centers for Environmental Information (NCEI) at https://data.nodc.noaa.gov/cgi-bin/iso?id=gov.noaa.nodc:0218215.

References

Anderson, E., Fujisaki-Manome, A., Kessler, J., Lang, G., Chu, P., Kelley, J., et al. (2018). Ice forecasting in the next-generation Great Lakes Operational Forecast System (GLOFS). *Journal of Marine Science and Engineering*, *6*(4), 123. https://doi.org/10.3390/jmse6040123

Austin, J. (2013). Observations of near-inertial energy in Lake Superior. *Limnology & Oceanography*, *58*(2), 715–728. https://doi.org/10.4319/lo.2013.58.2.0715

Austin, J., & Colman, S. (2008). A century of temperature variability in Lake Superior. *Limnology & Oceanography*, *53*(6), 2724–2730. https://doi.org/10.4319/lo.2008.53.6.2724

Austin, J. A., & Barth, J. A. (2002). Variation in the position of the upwelling front on the Oregon shelf. *Journal of Geophysical Research*, *107*(C11), 3180. https://doi.org/10.1029/2001JC000858

Austin, J. A., & Lentz, S. J. (2002). The inner shelf response to wind-driven upwelling and downwelling. *Journal of Physical Oceanography*, *32*(7), 2171–2193. https://doi.org/10.1175/1520-0485(2002)032<2171:TISRTW>2.0.CO;2

Ayers, J. C. (1956). A dynamic height method for the determination of currents in deep lakes. *Limnology & Oceanography*, *1*(3), 150–161. https://doi.org/10.4319/lo.1956.1.3.0150

Bai, P., Wang, J., Chu, P., Hawley, N., Fujisaki-Manome, A., Kessler, J., et al. (2020). Modeling the ice-attenuated waves in the Great Lakes. *Ocean Dynamics*, *70*, 991–1003. https://doi.org/10.1007/s10236-020-01379-z

Bai, X., Wang, J., Schwab, D. J., Yang, Y., Luo, L., Leshkevich, G. A., & Liu, S. (2013). Modeling 1993–2008 climatology of seasonal general circulation and thermal structure in the Great Lakes using FVCOM. *Ocean Modelling*, *65*, 40–63. https://doi.org/10.1016/j.ocemod.2013.02.003

Beletsky, D., Hawley, N., & Rao, Y. R. (2013). Modeling summer circulation and thermal structure of Lake Erie. *Journal of Geophysical Research: Oceans*, *118*, 6238–6252. https://doi.org/10.1002/2013JC008854

Beletsky, D., O'Connor, W. P., Schwab, D. J., & Dietrich, D. E. (1997). Numerical simulation of internal Kelvin waves and coastal upwelling fronts. *Journal of Physical Oceanography*, *27*(7), 1197–1215. https://doi.org/10.1175/1520-0485(1997)027<1197:NSOIKW>2.0.CO;2

Beletsky, D., Saylor, J. H., & Schwab, D. J. (1999). Mean circulation in the Great Lakes. *Journal of Great Lakes Research*, *25*(1), 78–93. https://doi.org/10.1016/S0380-1330(99)70718-5

Bennington, V., McKinley, G. A., Kimura, N., & Wu, C. H. (2010). General circulation of Lake Superior: Mean, variability, and trends from 1979 to 2006. *Journal of Geophysical Research*, *115*, C12015. https://doi.org/10.1029/2010JC006261

Brink, K. H. (2016). Cross-shelf exchange. *Annual Review of Marine Science*, *8*(1), 59–78. https://doi.org/10.1146/annurev-marine-010814-015717

Chen, C., Beardsley, R., & Cowles, G. (2006). An unstructured grid, Finite-Volume Coastal Ocean Model (FVCOM) system. *Oceanography*, *19*, 78–89. https://doi.org/10.5670/oceanog.2006.92

Chen, C., Beardsley, R. C., Cowles, G., Qi, J., Lai, Z., Gao, G., et al. (2013). *An unstructured grid, Finite-Volume Community Ocean Model FVCOM user manual, SMAST/UMASSD-13-0701* (Tech. Rep., p. 416). New Bedford, MA: School for Marine Science & Technology, University of Massachusetts Dartmouth.

Chen, C., Liu, H., & Beardsley, R. C. (2003). An unstructured grid, finite-volume, three-dimensional, primitive equations ocean model: Application to coastal ocean and estuaries. *Journal of Atmospheric and Oceanic Technology*, *20*(1), 159–186. https://doi.org/10.1175/1520-0426(2003)020<0159:AUGFVT>2.0.CO;2

Chen, C., Xu, Q., Ralph, E., Budd, J. W., & Lin, H. (2004). Response of Lake Superior to mesoscale wind forcing: A comparison between currents driven by QuikSCAT and buoy winds. *Journal of Geophysical Research*, *109*, C10S02. https://doi.org/10.1029/2002JC001692

Chen, C., Zhu, J., Kang, K., Liu, H., Ralph, E., Green, S. A., & Budd, J. W. (2002). Cross-frontal transport along the Keweenaw coast in Lake Superior: A Lagrangian model study. *Dynamics of Atmospheres and Oceans*, *36*(1), 83–102. https://doi.org/10.1016/S0377-0265(02)00026-X

Chen, C., Zhu, J., Ralph, E., Green, S. A., Budd, J. W., & Zhang, F. Y. (2001). Prognostic modeling studies of the Keweenaw current in Lake Superior. Part I: Formation and evolution. *Journal of Physical Oceanography*, *31*(2), 379–395. https://doi.org/10.1175/1520-0485(2001)031<0379:PMSOTK>2.0.CO;2

Csanady, G. T. (1977). Intermittent 'full' upwelling in Lake Ontario. *Journal of Geophysical Research*, *82*(3), 397–419. https://doi.org/10.1029/JC082i003p00397

Csanady, G. T. (1982). *Circulation in the coastal ocean*. Dordrecht, The Netherlands: Springer. https://doi.org/10.1007/978-94-017-1041-1

Fujisaki-Manome, A., & Wang, J. (2016). *Simulating hydrodynamics and ice cover in Lake Erie using an unstructured grid model*. Paper presented at Proceedings of 23th IAHR International Symposium on Ice, Ann Arbor, Michigan, May 31 to June 3, 2016.

Hu, H., & Wang, J. (2010). Modeling effects of tidal and wave mixing on circulation and thermohaline structures in the Bering Sea: Process studies. *Journal of Geophysical Research*, *115*, C01006. https://doi.org/10.1029/2008JC005175

Hunke, E. C., & Dukowicz, J. K. (1997). An elastic–viscous–plastic model for sea ice dynamics. *Journal of Physical Oceanography*, *27*(9), 1849–1867. https://doi.org/10.1175/1520-0485(1997)027<1849:AEVPMF>2.0.CO;2

Jerlov, N. G. (1968). *Optical oceanography*. New York: American Elsevier Publishing Co., Inc.

Jerlov, N. G. (1976). Marine optics (2nd ed., 14). Amsterdam, The Netherlands: Elsevier Science. Retrieved from https://www.elsevier.com/books/marine-optics/jerlov/978-0-444-41490-8

Kirillin, G., & Shatwell, T. (2016). Generalized scaling of seasonal thermal stratification in lakes. *Earth-Science Reviews*, *161*, 179–190. https://doi.org/10.1016/j.earscirev.2016.08.008

Large, W. G., & Pond, S. (1981). Open ocean momentum flux measurements in moderate to strong winds. *Journal of Physical Oceanography*, *11*, 324–336.

Large, W. G., & Pond, S. (1982). Sensible and latent heat flux measurements over the ocean. *Journal of Physical Oceanography*, *12*(5), 464–482. https://doi.org/10.1175/1520-0485(1982)012<0464:SALHFM>2.0.CO;2

Mellor, G., & Blumberg, A. (2004). Wave breaking and ocean surface layer thermal response. *Journal of Physical Oceanography*, *34*(3), 693–698. https://doi.org/10.1175/2517.1

Mellor, G. L. (2001). One-dimensional, ocean surface layer modeling: A problem and a solution. *Journal of Physical Oceanography*, *31*(3), 790–809. https://doi.org/10.1175/1520-0485(2001)031<0790:ODOSLM>2.0.CO;2

Mellor, G. L., & Yamada, T. (1982). Development of a turbulence closure model for geophysical fluid problems. *Reviews of Geophysics*, *20*(4), 851–875. https://doi.org/10.1029/RG020i004p00851

Mesinger, F., DiMego, G., Kalnay, E., Mitchell, K., Shafran, P. C., Ebisuzaki, W., et al. (2006). North American Regional Reanalysis. *Bulletin of the American Meteorological Society*, *87*(3), 343–360. https://doi.org/10.1175/BAMS-87-3-343

Monismith, S. (1986). An experimental study of the upwelling response of stratified reservoirs to surface shear stress. *Journal of Fluid Mechanics*, *171*, 407–439. https://doi.org/10.1017/S0022112086001507

Niebauer, H. J., Green, T., & Ragotzkie, R. A. (1977). Coastal upwelling/downwelling cycles in southern Lake Superior. *Journal of Physical Oceanography*, *7*, 918–927. https://doi.org/10.1175/1520-0485(1977)007<0918:CUCISL>2.0.CO;2

Paulson, C. A., & Simpson, J. J. (1977). Irradiance measurements in the upper ocean. *Journal of Physical Oceanography*, *7*(6), 952–956. https://doi.org/10.1175/1520-0485(1977)007<0952:IMITUO>2.0.CO;2

Plattner, S., Mason, D. M., Leshkevich, G. A., Schwab, D. J., & Rutherford, E. S. (2006). Classifying and forecasting coastal upwellings in Lake Michigan using satellite derived temperature images and buoy data. *Journal of Great Lakes Research*, *32*(1), 63–76. https://doi.org/10.3394/0380-1330%282006%2932%5B63%3ACAFCUI%5D2.0.CO%3B2

Qiao, F., Yuan, Y., Yang, Y., Zheng, Q., Xia, C., & Ma, J. (2004). Wave-induced mixing in the upper ocean: Distribution and application to a global ocean circulation model. *Geophysical Research Letters*, *31*, L11303. https://doi.org/10.1029/2004GL019824

Roberts, D. C., Egan, G. C., Forrest, A. L., Largier, J. L., Bombardelli, F. A., Laval, B. E., et al. (2021). The setup and relaxation of spring upwelling in a deep, rotationally influenced lake. *Limnology & Oceanography*, *66*(4), 1168–1189. https://doi.org/10.1002/lno.11673

Schladow, S. G., Pálmarsson, S. Ó., Steissberg, T. E., Hook, S. J., & Prata, F. E. (2004). An extraordinary upwelling event in a deep thermally stratified lake. *Geophysical Research Letters*, *31*, L15504. https://doi.org/10.1029/2004GL020392

Schwab, D. J., & Bedford, K. W. (1999). *The Great Lakes forecasting system*. https://doi.org/10.1029/ce056p0157

Schwab, D. J., Leshkevich, G. A., & Muhr, G. C. (1999). Automated mapping of surface water temperature in the Great Lakes. *Journal of Great Lakes Research*, *25*(3), 468–481. https://doi.org/10.1016/S0380-1330(99)70755-0

Simons, T. J., & Schertzer, W. M. (1987). Stratification, currents, and upwelling in Lake Ontario, summer 1982. *Canadian Journal of Fisheries and Aquatic Sciences*, *44*, 2047–2058. https://doi.org/10.1139/f87-254

Smagorinsky, J. (1963). General circulation experiments with the primitive equations. *Monthly Weather Review*, *91*(3), 99–164. https://doi.org/10.1175/1520-0493(1963)091<0099:GCEWTP>2.3.CO;2

Smith, R. L. (1995). The physical processes of coastal ocean upwelling systems. In C. P. Summerhayes, et al. (Eds.), *Upwelling in the ocean: Modern processes and ancient records* (pp. 39–64). Chichester, UK: John Wiley and Sons.

Titze, D. J., & Austin, J. A. (2014). Winter thermal structure of Lake Superior. *Limnology & Oceanography*, *59*(4), 1336–1348. https://doi.org/10.4319/lo.2014.59.4.1336

Wang, J. (1996). Global linear stability of the two-dimensional shallow-water equations: An application of the distributive theorem of roots for polynomials on the unit circle. *Monthly Weather Review*, *124*(6), 1301–1310.

Wang, J., & Ikeda, M. (1997a). Diagnosing ocean unstable baroclinic waves and meanders using the quasigeostrophic equations and Q-vector method. *Journal of Physical Oceanography*, *27*(6), 1158–1172.

Wang, J., & Ikeda, M. (1997b). Inertial stability and phase error of time integration schemes in ocean general circulation models. *Monthly Weather Review*, *125*(9), 2316–2327.

White, B., Austin, J., & Matsumoto, K. (2012). A three-dimensional model of Lake Superior with ice and biogeochemistry. *Journal of Great Lakes Research*, *38*(1), 61–71. https://doi.org/10.1016/j.jglr.2011.12.006

Wyrtki, K. (1965). The average annual heat balance of the North Pacific Ocean and its relation to ocean circulation. *Journal of Geophysical Research*, *70*(18), 4547–4559. https://doi.org/10.1029/JZ070i018p04547

Ye, X., Anderson, E. J., Chu, P. Y., Huang, C., & Xue, P. (2019). Impact of water mixing and ice formation on the warming of Lake Superior: A model-guided mechanism study. *Limnology & Oceanography*, *64*(2), 558–574. https://doi.org/10.1002/lno.11059

Yuan, Y., Qiao, F., Hua, F., & Wan, Z. (1999). The development of a coastal circulation numerical model. 1. Wave-induced mixing and wave–current interaction [in Chinese with English abstract]. *Journal of Hydrodynamics Series A*, *14*, 1–8.

Zhu, J., Chen, C., Ralph, E., Green, S. A., Budd, J. W., & Zhang, F. Y. (2001). Prognostic modeling studies of the Keweenaw current in Lake Superior. Part II: Simulation. *Journal of Physical Oceanography*, *31*(2), 396–410. https://doi.org/10.1175/1520-0485(2001)031<0396:PMSOTK>2.0.CO;2